GEOLOGY

Direct dating of lithic surface artifacts using luminescence

Luke Andrew Gliganic[1]*†, Michael Christian Meyer[1]*, Jan-Hendrik May[2], Mark Steven Aldenderfer[3], Peter Tropper[4]

Archaeological surface assemblages composed of lithic scatters comprise a large proportion of the archaeological record. Dating such surface artifacts has remained inherently difficult owing to the dynamic nature of Earth-surface processes affecting these assemblages and because no satisfactory chronometric dating technique exists that can be directly applied to constrain the timing of artifact manufacture, discard, and thus human use of the landscape. Here, we present a dating approach based on optically stimulated luminescence (OSL)—OSL rock-surface burial dating—and apply it to a lithic surface scatter in Tibet. We generate OSL burial ages (age-depth profiles) for each artifact, outline the methodological complexities, and consider the artifact burial ages in the context of local-scale Earth-surface dynamics. The oldest age cluster between 5.2 and 5.5 thousand years is likely related to quarrying activities at the site and thus represents the oldest chronometric age constraints for human presence on the south-central Tibetan plateau.

INTRODUCTION

Humans and their ancestors have been making stone tools for millions of years. Sites composed of the by-products of tool production and use are among the most commonly encountered sites in the archaeological record around the world. Frequently, these artifacts occur on or near the ground surface. Such anthropogenically formed surface lithic artifact scatter sites are notoriously difficult to place into a reliable chronological framework because (i) organic materials that can be radiocarbon-dated and that are directly associated with these finds are often lacking and (ii) such scatter sites may not be composed of artifact types diagnostic of an unequivocal temporal period. Furthermore, there are very few archaeometric techniques available to date worked stone directly. Without age control, it is difficult to use these assemblages to reconstruct settlement patterns, infer social relationship, and explore other aspects of human behavior in the past (*1*, *2*).

The only methods currently available for direct chronometric dating of lithic artifacts are thermoluminescence and obsidian hydration dating. However, both techniques come with serious methodological limitations that constrain either the range of applications or the reliability of each method (*3*, *4*). In addition, a range of Earth-surface processes can also modify the pattern and stratigraphic position of lithic surface artifacts and thus affect the landscape context of such assemblages and their interpretation [e.g., (*5*–*9*)]. Therefore, any attempt to directly constrain the chronology of lithic surface artifacts and/or stone tools, and to glean archaeologically meaningful interpretations from such surface assemblages, requires that the type and dynamic nature of geomorphic surface processes are adequately accounted for (*9*, *10*).

Promising recent work has shown the potential of using the optically stimulated luminescence (OSL) signal from rock surfaces to date the emplacement of gravel pavements and blocks in both archaeological (*11*–*13*) and geological contexts (*14*, *15*). OSL rock-surface dating has also been used to constrain the exploitation of a lithic raw material quarry (*16*) and the timing of a whetstone usage (*17*). These variants of OSL rock-surface dating either (i) use the degree of OSL signal resetting (bleaching) into a rock surface as a measure of exposure time [i.e., rock-surface exposure dating; e.g., (*16*, *17*)] or (ii) measure the reaccumulated luminescence signal from formerly bleached gravel or boulder surfaces to obtain rock burial ages. The latter approach, known as rock-surface burial dating, can be applied to, for example, the light-shielded undersides of subaerially exposed rocks [e.g., (*11*–*14*)] or to gravels that have been partly bleached and subsequently completely buried (*15*).

Here, we apply OSL rock-surface burial dating to provide age control for a surface lithic artifact scatter at the Su-re site in south-central Tibet and demonstrate its usefulness in establishing temporal frameworks for archaeological surface deposits. Specifically, we (i) show that the OSL signal in our samples bleaches during sunlight exposure, (ii) calculate OSL burial ages for slices at 1-mm increments into each artifact's buried surface (i.e., age-depth profiles into the artifact's interior), and (iii) determine ages for the last exposure of these artifact surfaces to sunlight. The resulting OSL ages are used to infer the timing of artifact discard by humans at the site while simultaneously inferring events of erosion, transport, and renewed deposition since initial site creation. In this case, our spatially resolved OSL burial ages (age-depth profiles) help to constrain the timing and the number of cycles of artifact burial and re-exhumation. Therefore, our novel approach holds great potential to date sunlight exposure of lithic artifacts and gain information on post-depositional disturbances and transport pathways that is ultimately required to reconstruct more complete site-specific artifact histories.

Study area: The Su-re lithic artifact scatter on the southern Tibetan plateau

In the arid high-altitude setting of the Tibetan plateau, organic material for radiocarbon dating is scarce and deeply stratified sites are

[1]Institute for Geology, University of Innsbruck, Innrain 52, 6020 Innsbruck, Austria. [2]School of Geography, University of Melbourne, 221 Bouverie St, Carlton, VIC 3053, Australia. [3]Department of Anthropology and Heritage Studies, University of California, Merced, CA 95343, USA. [4]Institute for Mineralogy and Petrography, University of Innsbruck, Innrain 52, 6020 Innsbruck, Austria.
*Corresponding author. Email: luke.gliganic@gmail.com (L.A.G.); michael.meyer@uibk.ac.at (M.C.M.)
†Present address: Centre for Archaeological Science, School or Earth, Atmospheric and Life Sciences, University of Wollongong, Northfields Avenue, Wollongong, NSW 2500, Australia.

extremely rare, partly because morphodynamic processes are operating at low intensity and rates. In contrast, lithic assemblages and broken ceramics are frequently encountered on the surface of various landscape elements including hillslopes, fluvial terraces, and beach ridges as well as in the vicinity of thermal springs (*18*–*23*). Archaeological surface assemblages on the Tibetan plateau generally lack reliable artifact types diagnostic of temporal periods, thus posing challenges to building accurate chronologies of past behavioral processes. We chose an archaeological site in south-central Tibet—known as Su-re—that is characterized by surface artifacts (*24*, *25*) to develop and test our OSL rock-surface dating approach for surface lithic artifact discard.

Su-re is a lithic artifact scatter associated with a lithic quartzite quarry located to the north of the Mount Everest-Cho Oyu massif (Fig. 1, A and B). The site is situated on a south-facing hillside on the eastern shoulder of the Tingri Graben at an elevation of 4450 meters above sea level [Figs. 1B and 2A; (*16*, *23*)]. A 5806-m high and glaciated mountain pass (Nangpa La) that connects the Tingri area with the Khumbu Himalaya of Nepal is approximately 50 km south of Su-re. The Nangpa La historically served as a trade and pilgrimage route connecting the local Tibetans and Nepali Sherpas until 1950 and may have been a link between the Tibetan Plateau and the southern Himalayan lowlands in prehistory (*23*, *26*, *27*).

The Su-re hill comprises lithified sediments of the Tibetan sedimentary sequence including Paleozoic to Cenozoic fossiliferous sandstones and siltstones, limestones, and shales, and is capped by a meters-thick quartzite unit (*28*). Quartzite boulders have accumulated at the base of a debris-covered slope that has an average gradient of ~40% (Fig. 2B). These quartzite boulders likely moved down from the capping unit via periglacial mass-wasting processes (*23*). The boulders exhibit negative flake scars (*16*) and are surrounded by lithic debris among naturally occurring gravel-sized clasts (Fig. 2, D and E, and figs. S1 and S2). All cores and the vast majority of flakes are of the local quartzite raw material, with all observed archaeological material being associated with the exploitation of the quarry. None of these reduction by-products have chronologically diagnostic attributes. The hillslope area over which these quartzite boulders and artifacts occur has an average gradient of ~15%, is ~1.4 ha in area, and extends for several hundred meters in a northwest-southeast direction (Fig. 2A). Linear gully incision and sheetwash erosion occur on this gently inclined and lithic-strewn section of the Su-re hillside (Fig. 2B and fig. S3). Furthermore, an aeolian cover sand, 0.2 to 1.8 m in thickness and OSL dated to ca. 0.56 ± 0.08 thousand years (ka) (*23*), drapes wide areas of the hillslopes and the adjacent fluvial terraces. This cover sand shows signs of intensive degradation mainly by wind erosion (Fig. 2, A and B). The aeolian cover sand rests disconformably on a mid-Holocene pedo-complex that is expressed as a marked reddish weathering (Bv) horizon in the Su-re area (*23*). The artifacts come from a slope area that is dominated by slope wash processes where no or only a very thin veneer of aeolian cover sands are preserved (Fig. 2A). All artifacts rest stratigraphically atop the mid-Holocene pedo-complex, although some artifacts were found semi-embedded in the remnants of a much younger aeolian cover sand or a thin veneer of slope-wash sediment (figs. S2 and S3). None of the artifacts show signs of intentional heat alteration and the lithic raw material at Su-re is probably also not amenable to this type of modification (*29*). Evidence for post-depositional burning and thus unintentional heat alteration of the artifacts is absent too.

Approach

OSL dating is typically used to estimate the amount of time since sediment grains were last exposed to sunlight and subsequently buried (*30*, *31*). In short, the method relies on (i) the bleaching of the accumulated latent-OSL signal from sediment grains during light exposure and (ii) exposure to environmental radiation during burial and consequent accumulation of the latent-OSL signal in buried grains (*31*). The same principles allow the OSL signal to be used for dating the sunlight exposure and subsequent burial of quartz- or K-feldspar–rich rock surfaces [rock-surface burial dating; e.g., (*15*, *17*)]. In this study, we are interested in when a quartzite artifact (i.e., a by-product of lithic reduction) was last created and subsequently discarded because it allows us to temporally constrain lithic surface assemblages and thus site use. The principle of such a rock-surface burial dating approach applied to lithic surface artifacts is outlined in Fig. 3. Stone tools are created by removing lithic raw material from a quarry and shaping the resulting mass (i.e., a core)

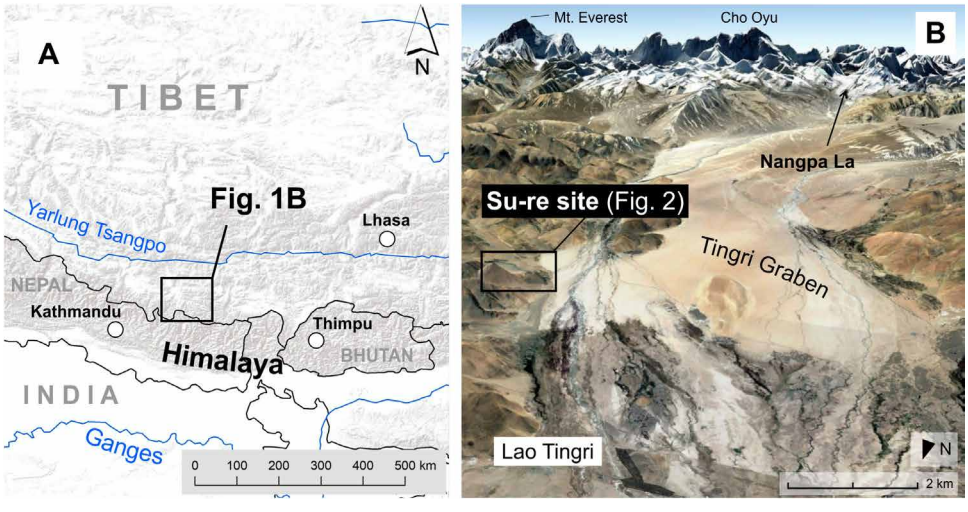

Fig. 1. Geographical setting of the studied site. (**A**) Location of the Tingri Graben in the Himalaya. (**B**) Google Earth perspective of the Tingri Graben and the high Himalaya viewing roughly south indicating the location of the Su-re archaeological site. Photo credit: (B) Google Earth image.

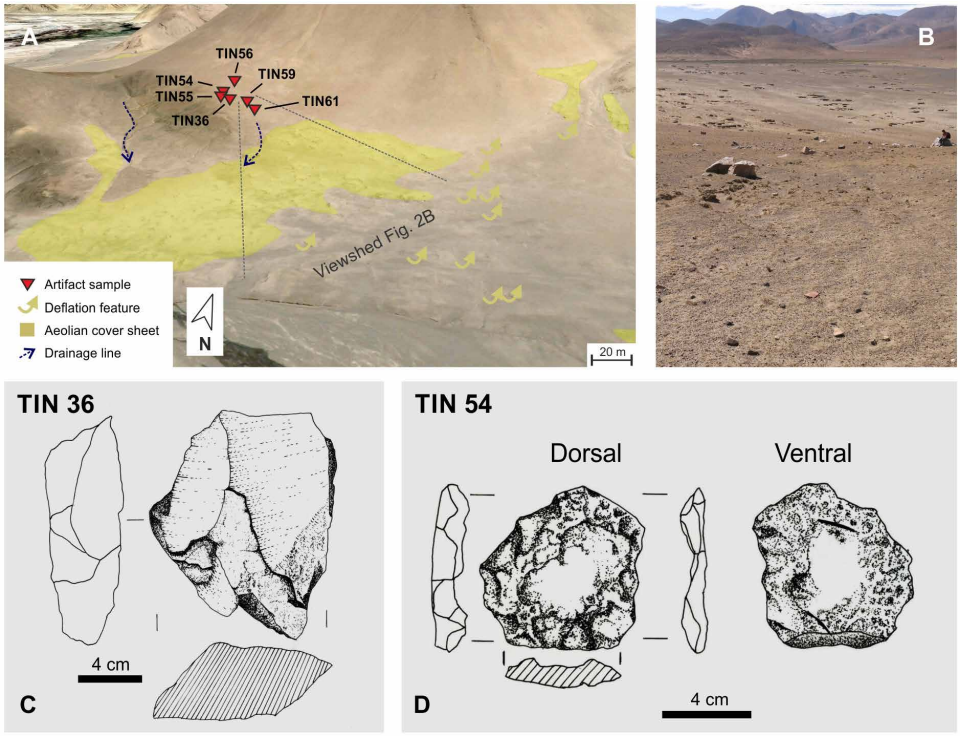

Fig. 2. Features of the Su-re archaeological site. (**A**) Google Earth oblique aerial view with positions of sampled surface artifacts along the hillslope at Su-re (view is to the northwest). (**B**) View over the lithic surface scatter site into the Su-re valley with large quartzite boulders that have been partly quarried (middle ground of image). Note the degraded aeolian cover sands in the background and shallow drainage lines from the concentration of overland flow in the foreground. (**C** and **D**) Detailed sketch of artifact TIN36 and TIN54, respectively. Photo credit: (A) Google Earth image; (B) M. C. Meyer, University of Innsbruck.

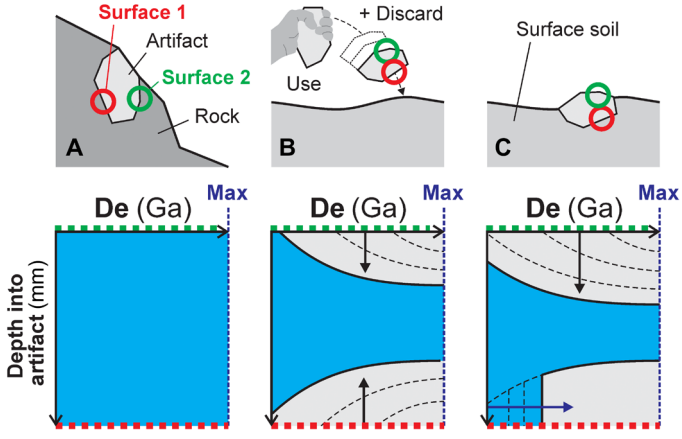

Fig. 3. Conceptual model showing the dating approach highlighting a common pathway of a lithic artifact in the landscape and the corresponding changes to the luminescence signal on the object surface of interest. (**A**) Artifact still in its original bedrock context before exposure by quarrying and/or knapping. (**B**) Artifact use and/or discard by humans leading to exposure and bleaching of the luminescence signal on all surfaces. (**C**) Artifact settling, embedding, and semiburial in the soil leading to luminescence signal buildup (red and green dotted lines indicate two opposing artifact surfaces). Note that exposure of an air-facing artifact surface before knapping (i.e., prior exposure, while still "in situ" in the quarry setting) such as in (A) will contribute to the bleaching of the artifact surfaces that continues in (B).

into a desired shape. In doing so, many new rock surfaces are created and exposed to sunlight throughout the process of stone-tool preparation (Fig. 3, A and B). Through the lifetime of an artifact, i.e., over the period of usage, the surfaces exposed to sunlight will have their latent-OSL signals bleached until they become shielded or partially shielded from sunlight by burial or discard, after which the latent-OSL signal will begin accumulating at a rate proportional to the equivalent dose (De) rate in the rock itself, from the surrounding sediment, and cosmic rays (Fig. 3C; semi-embedded artifact is bleached from the top while latent-OSL signal accumulates at light-shielded underside). For reduction by-products such as lithic flakes and debris, not all artifact surfaces might be bleached sufficiently because such lithics are discarded rapidly at an early stage of stone-tool fabrication or were generated by nodule testing. Conversely, prior exposure of the quarry rock surface can contribute to the bleaching of an artifact while still in situ, if the artifact surface was built directly from the quarry rock surface without modification (Fig. 3A).

As discussed below, even more complex burial and bleaching histories can potentially be recorded by a single artifact (see 'Dating artifact discard'). Therefore, obtaining a good understanding of the bleaching properties of the artifact material is crucial. First, it must be demonstrated that the grains that comprise the artifact can have their geologically inherited OSL signals reset by natural sunlight. Then, to unravel and interpret the burial and bleaching history, highly resolved spatial measurements of the OSL signal into the artifact surface are required.

Six lithic artifacts collected from semi-embedded contexts in the vicinity of the quarried quartzite boulders at Su-re were investigated for this study (Fig. 2, D and E, and figs. S1 and S2). Each is a large primary decortication flake. Of these, four (TIN54, TIN56, TIN59, and TIN61) have well-defined striking platforms with pronounced bulbs of percussion and have abrupt and angular terminations from the parent material. The dorsal surface of each is fully covered with a weathered cortex. None of these four has additional dorsal scarring. TIN59, in contrast, has a broad, wide platform, but the bulb of percussion sheared off as the flake was removed from the parent material. This artifact also has an abrupt, angular termination from the parent material. Its dorsal surface has two large flake scars that have removed roughly 50% of the cortex. Last, TIN36 is a massive, blocky decortication flake with a shattered platform and irregular bulb of percussion. Its dorsal surface, 75% covered with cortex, exhibits two large flake scars that may have been produced when the flake was detached given their angular shape.

All artifacts were at least partially embedded in the surrounding sediment, indicating that they were not recently moved or flipped by natural processes. In light-safe conditions (under an opaque tent with red-light illumination), the artifacts were excavated, labeled, described, and wrapped in opaque material for transport to the laboratory. Sediment samples directly underlying each artifact were collected for dosimetry measurements.

In the laboratory, cores (~10 mm diameter) were collected from the buried face of each artifact using a small-diameter diamond core drill. The cores were sliced in 1-mm increments using a Buehler water-cooled low-speed saw with a 300-μm-thick blade, yielding ~0.7-mm-thick slices. Slices were crushed using a mortar and pestle and sieved to retain grains of 90- to 250-μm diameter. Between four and six aliquots comprising ~600 grains (5-mm mask size) were then mounted and De values were measured for each slice (see Materials and Methods). Environmental dose rates were measured for each artifact and an underlying sediment sample individually using a combination of methods including thick-source alpha counting, beta counting, mass and optical emission spectrometry, modeling (*32*), and in situ dose-rate measurement with aluminum oxide chips. For selected samples, petrographic thin-section and electron probe microanalysis (EPMA) were conducted to check artifact internal mineralogical and radionuclide distributions and thus dose rates (fig. S4). Spatially relevant dose rates were calculated for each slice (see Materials and Methods), and the resulting OSL age-depth profiles into the buried surface were used to (i) estimate OSL burial ages for the buried face of the artifact and (ii) identify whether the artifact has experienced multiple daylight exposure and burial events since discard (*11*, *33*).

RESULTS

Testing the bleachability of Su-re quartzite

The bleachability of the Su-re quartzite has been investigated by Gliganic *et al.* (*16*) in the course of their OSL rock-surface exposure dating approach that has been applied to the negative flake scars found on several Su-re quartzite boulders. We build on these data and generate new data that are relevant for our rock-surface burial dating approach to provide age control for the Su-re artifact scatter. The bleaching tests of Gliganic *et al.* (*16*) and our new data that are based on the same previous bleaching tests are both described here to provide the relevant background information for understanding the concept and importance of these bleaching tests in the context of OSL burial dating of lithic artifacts.

Gliganic *et al.* (*16*) conducted two bleaching experiments, involving geologically saturated quartzite samples being either (i) stimulated with light from a solar simulator in a laboratory setting or (ii) exposed to natural sunlight in the field for a known amount of time. For the laboratory experiment, six cubes of geologically saturated Su-re quartzite material were exposed to solar simulator light for varying durations ranging from 0 (control) to 1040 ks (~12 days). Cores were then drilled into the exposed surfaces, the cores were sliced in 1-mm increments, and slices were crushed to grains. The quartz grains were mounted on stainless steel discs using silicon spray (~600 grains per aliquot), and sensitivity-corrected measurements of the natural luminescence signal (i.e., Ln/Tn measurements) were made to construct OSL-depth profiles (*16*). From the shape of these Ln/Tn-based OSL-depth profiles, Gliganic *et al.* (*16*) ultimately derived rock-surface exposure ages. Here, we pursue a rock-surface burial dating approach and, hence, are concerned with (re-)accumulated burial doses in formerly bleached artifact surfaces (see Fig. 3). Consequently, to assess the bleaching and quantify any remaining residual dose after bleaching, the Ln/Tn values need to be converted to De values. We achieve this by generating a standardized growth curve (SGC) (*34*) based on the measurement of 372 aliquots of Su-re quartzite material. De values are plotted against depth in Fig. 4 (A and B). After 10 ks of solar simulator exposure, the first slice (~2-mm depth) is bleached such that it yields a De value consistent with 0 Gy. After 100 ks of exposure, the first three slices (~4-mm depth) are bleached.

For the bleaching experiment under natural light conditions, two fresh rock surfaces were generated by Gliganic *et al.* (*16*) by chiseling off ~10-cm-thick rock slices from two selected quartzite boulders at Su-re. Both rock surfaces were resampled 1.667 years (~603 days) later and their OSL-depth profiles were determined as previously described (*16*). We converted these OSL-depth profiles into De-depth curves using the Su-re SGC. De values are plotted against depth in Fig. 4 (C and D). After 1.667 years of sunlight exposure at the Su-re site, the quartzite material is bleached to a depth of ~10 mm in the TIN2016-099 sample and to a depth of ~9 mm in the TIN2016-152 sample, with an average residual De of 0.8 Gy.

Data from these two bleaching experiments support the conclusion that the quartzite material from which all artifacts at Su-re are derived is easily bleached by sunlight. Assuming a solar simulator-to-sunlight insolation conversion factor of 3.3 (*35*), the data indicate that a fresh surface in geological saturation would be bleached to a depth of ~4 mm after ca. 963 hours of continuous sunlight exposure on the Tibetan plateau, which is roughly equivalent to 160 cloudless days in southern Tibet (*36*). Likewise, after 1.667 years, the fresh surface would be bleached to a depth of ~10 mm. Although natural and laboratory bleaching conditions are not directly comparable, these data indicate that, after the creation of a flake, any geologically saturated surfaces will be sufficiently bleached in a matter of months of sunlight exposure to reset the OSL signal in their surfaces.

However, the rapidity of bleaching in this quite translucent material also poses a problem. Thin flakes may be completely bleached through from above after discard, such that the grains comprising the buried surface may have their accumulating latent-OSL signal reset due to light penetration from the subaerially exposed side, effectively prohibiting any signal buildup. The negative flake scar of

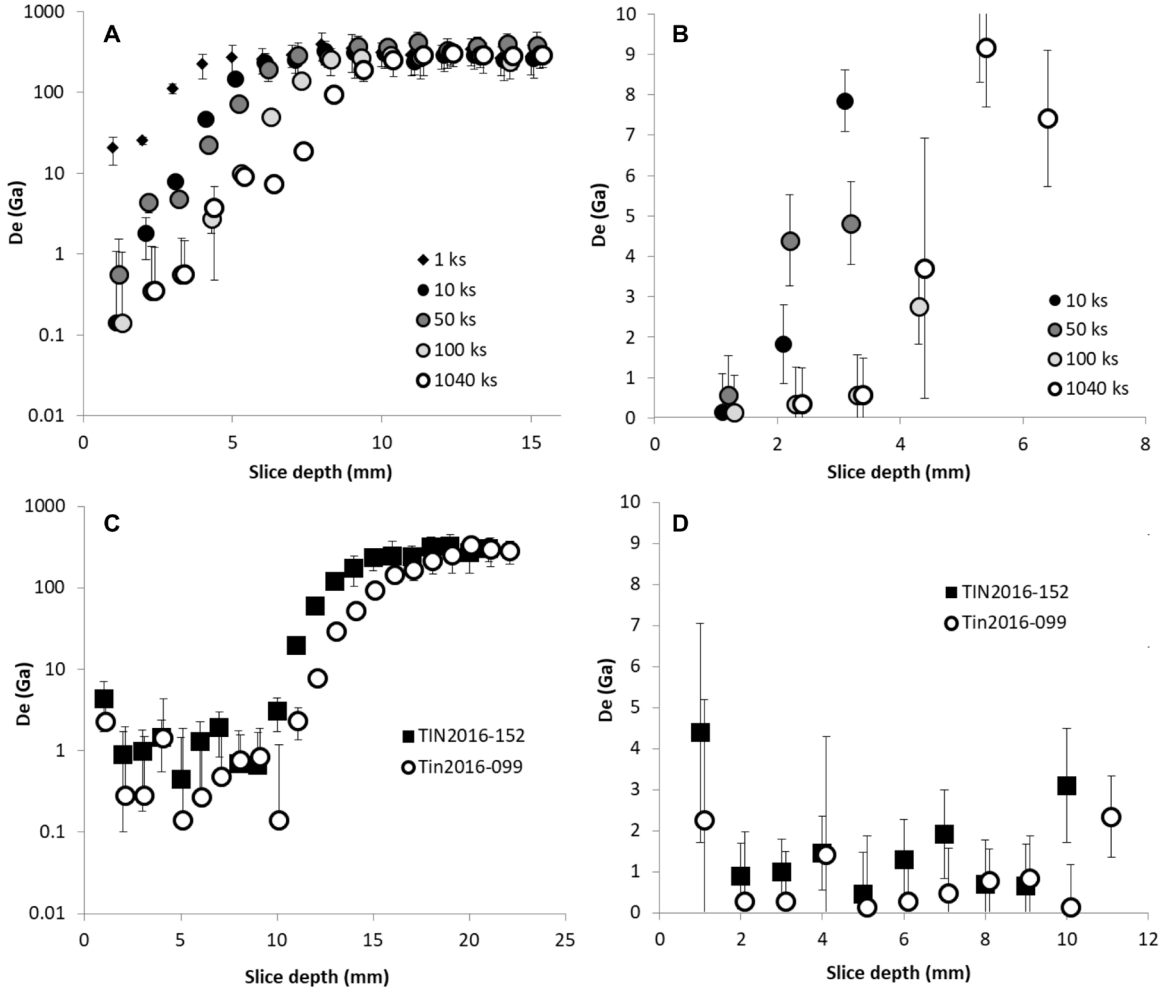

Fig. 4. De-depth profiles for the Su-re quartzite. (**A** and **B**) De-depth profiles for quartzite blocks exposed to a solar simulator for varying durations. (**C** and **D**) Daylight-bleached samples with a known exposure duration of 1.667 years. De-depth profiles are shown on a log-*y* scale (A and C) and on a linear scale [for values under 10 Gy: (B) and (D)] to visualize the depth to which material is bleached. Error bars indicate 1σ uncertainties.

one quartzite boulder sampled by Gliganic *et al.* (*16*) yielded an OSL-depth profile with the initial 21 mm of the scar surface completely bleached. These authors also determined the surface exposure age for this flake scar to 117 ± 35 years, and forward modeling of the bleaching properties of this specific quartzite scar sample indicates that, after 10 ka, the OSL signal would be bleached to within 5% of saturation to a depth of 43 mm into the surface (*16*). This issue emphasizes that flake thickness must be considered when sampling and analyzing surface artifacts and is kept in mind for interpreting the burial ages of the lithic scatter from Su-re.

Dating artifact discard

De values were measured for between four and six aliquots per slice for each sample. The weighted mean De value of aliquots from each slice was calculated using the central age model (CAM) (*37*) or the unlogged CAM where an aliquot yielded a negative De value (*38*), and spatially relevant dose rates were determined for each slice using the equations of Aitken (*32*) (appendix H), geomorphological field context, and sample morphology (table S1). The weighted mean De values and spatially relevant dose rates for each slice were then used to calculate spatially resolved burial ages, which were used to generate age-depth profiles for each artifact (Fig. 5).

In the previously discussed conceptual model (Fig. 3, A to C), an artifact has been bleached, discarded, and remained in situ in a semi-embedded context throughout its burial history. In this scenario, spatially resolved burial ages for the light-shielded underside of the artifact will correspond to the time of artifact discard, while ages are expected to increase toward the un-bleached interior of the artifact (Fig. 3C). Five of the six lithic samples from Su-re behave as expected, exhibiting the lowest ages closest to the buried surface and an increasing age profile with depth into the artifact (Fig. 5, A to E). Given this behavior, and the excellent bleachability of the quartzite material, it is expected that the OSL burial age of the slices closest to the surface will reflect the last time this surface was exposed to sunlight.

However, most samples reveal stepped rather than continuously increasing age-depth profiles, suggestive of a complex rather than simple burial and exposure history characterized by a prolonged period of shielding and renewed signal buildup beneath the formerly exposed surface (Fig. 6A). To better resolve the complexity of these

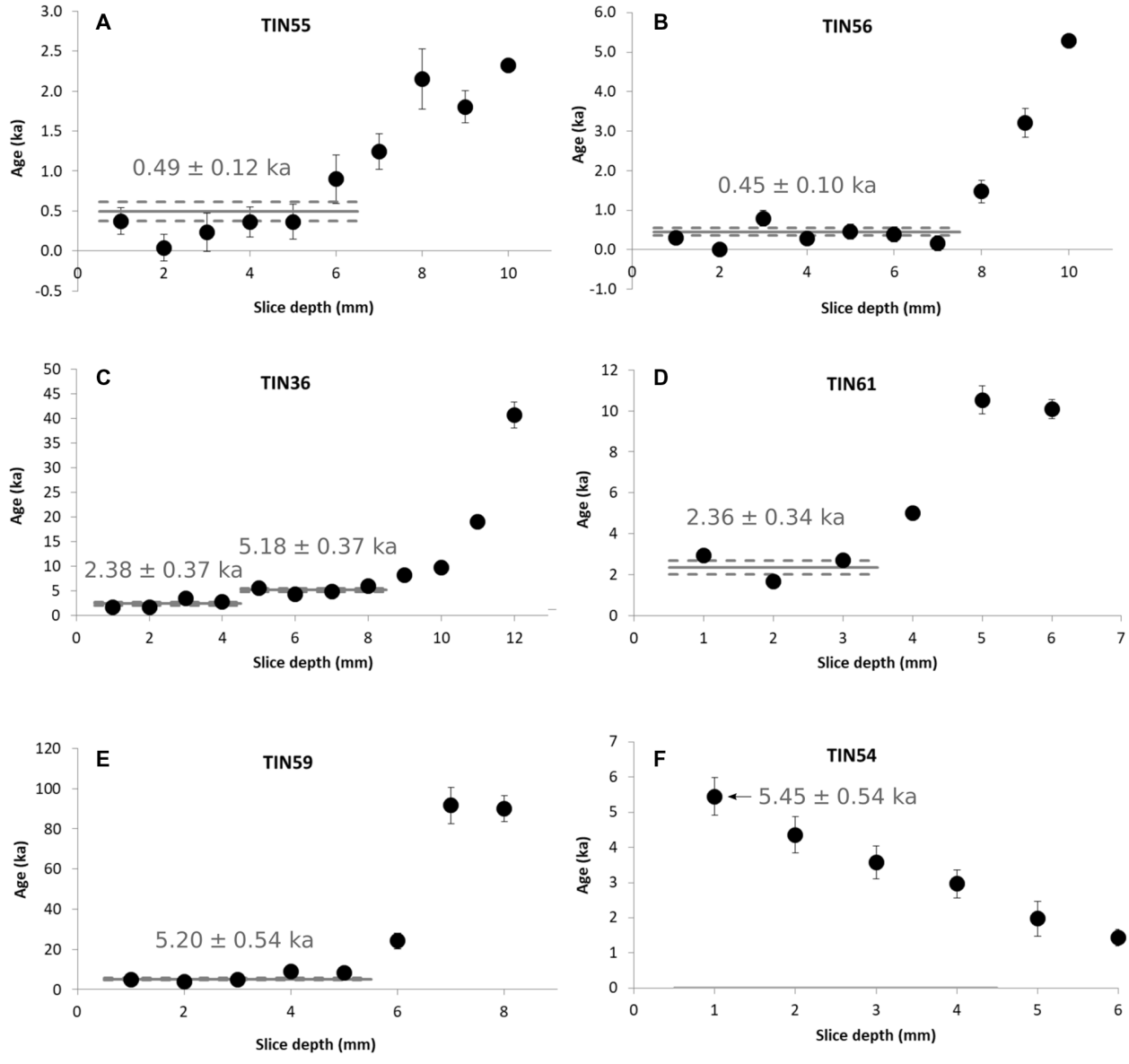

Fig. 5. Age-depth profiles showing age plateaus (solid lines) for all samples. (**A**) TIN55, (**B**) TIN56, (**C**) TIN36, (**D**) TIN61, (**E**) TIN59 , and (**F**) TIN54. The errors for the individual ages as well as for the burial age plateaus (dashed line) are plotted as 1σ errors. Sample TIN54 lacks an age plateau in an inverted age-depth profile due to nearly complete bleaching from above and thus yielded a minimum age of 5.45 ± 0.54 ka (for details, see the main text).

cases, the age-depth data for all samples were analyzed for plateaus using a simple statistical homogeneity test that identifies statistically consistent populations (*39*). The burial age for each artifact surface was then calculated using the CAM of all slice ages comprising their plateau. Three samples (TIN55, TIN56, and TIN59) exhibited the expected homogeneous plateaus in their age-depth profiles (Fig. 5, A, B, and E), indicating that a single exposure and burial event can best explain these data. This suggests that burial occurred at ~0.45 and 5.2 ka (Fig. 5). One sample (TIN61), however, exhibited a clear plateau that did not comprise a homogeneous population of ages (Fig. 5D), and for which the CAM was used, suggesting burial at ~2.36 ka.

The two remaining samples (TIN36 and TIN54) show more complex age-depth profiles. Two plateaus were identified in the TIN36 age-depth profile (Fig. 5C); slices 5 to 8 yield a weighted mean age of 5.18 ± 0.37 ka, while slices 1 to 4 yield a weighted mean age of 2.38 ± 0.37 ka. These data can be best explained as representing at least two bleaching and subsequent burial events (Fig. 6A). The first event bleached the surface to a depth of 8 mm before reburial at ~5.18 ka, which best approximates the age for artifact creation and discard. Subsequently, at ~2.38 ka, the surface was re-exposed for sufficient time to be bleached to a depth of 4 mm before subsequent reburial.

Sample TIN54 (Fig. 5F) exhibits an inverted age-depth profile, with the oldest slice age (5.45 ± 0.54 ka) at the surface and ages decreasing as depth increases. This profile indicates that the artifact has been bleached from the exposed surface above, a plausible scenario given the relative thinness (20 mm) of this artifact (Fig. 6B and

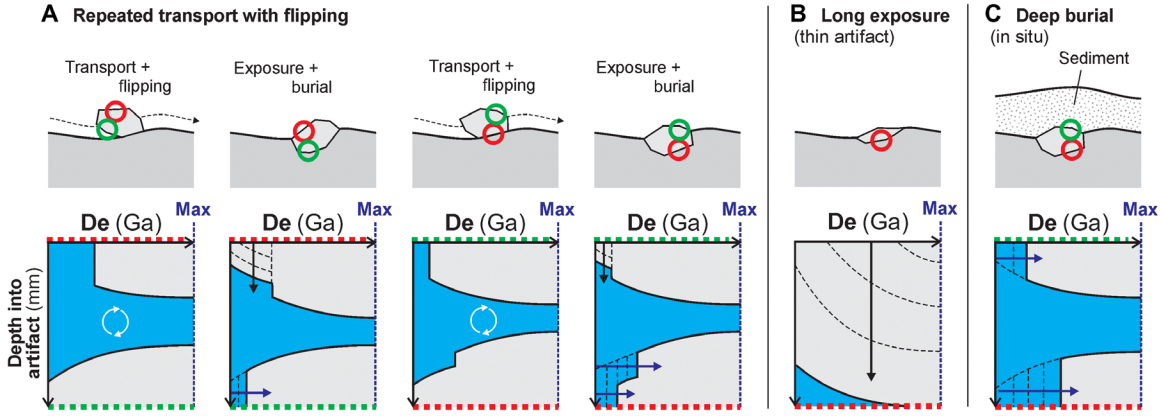

Fig. 6. Additional and more complex pathways of rock artifacts in the landscapes and the corresponding luminescence signal (note that all pathways continue from a semi-embedded artifact as shown in Fig. 3C). (**A**) Repeated transport with artifact flipping and subsequent shielding, (**B**) the case of a thin artifact subject to complete bleaching from the exposed surface, and (**C**) shielding by deep in situ burial (e.g., via aeolian deposition).

fig. S1). The most parsimonious explanation for the data is that the artifact was produced and bleached some time at or before ~5.45 ka, was then buried, and was subsequently exhumed and re-exposed.

DISCUSSION

The artifact burial ages presented here have a range of implications for better understanding site use at Su-re. They also provide an important step toward assessing the potential of using OSL burial dating in archaeological (or other) settings elsewhere.

Types and time scales of site use at Su-re

The artifact discard chronology includes two plateau ages with a weighted mean of 0.47 ± 0.08 ka (TIN55 and TIN56), two plateau ages with a weighted mean of 2.37 ± 0.25 ka (TIN36 and TIN61), two plateau ages with a weighted mean of 5.19 ± 0.31 ka (TIN36 and TIN59), and one minimum age of 5.45 ± 0.54 ka (TIN54). The plateau ages cover the time span from the mid- to the late Holocene, which is in agreement with the stratigraphic position of these artifacts atop a mid-Holocene pedo-complex (fig. S3).

While these lithic artifacts and the associated ages provide clear evidence for human presence at Su-re and human exploitation of the associated quarry site since at least the mid-Holocene, they also provide an opportunity to discuss the interpreted exposure and burial histories as well as the associated natural and anthropogenic processes within the local paleoenvironmental context (*23*). The mid-Holocene population of burial ages suggests the initial manufacture and use of these artifacts and the quartzite quarry sometime before ~5 ka (i.e., the set of oldest plateau ages from TIN36, TIN59, and TIN54), followed by discard and at least partial burial. While we cannot rule out that the most recent bleaching event recorded by these artifacts obliterated evidence of even earlier cycles of exposure and burial in the landscape, the most parsimonious interpretation of these oldest plateau ages invokes a simple exposure and burial scenario and a close temporal relationship between artifact manufacture, discard, and burial followed by longer-term stability without any further disturbance. Paleoenvironmental records indicate that the landscape at Su-re between ~6.7 and 3.9 ka was characterized by relative stability, with soils and wetlands forming (*23*). Palynomorphs extracted from these soils indicate locally to regionally moist conditions based on the presence of *Glomus*-type spores produced by soil fungi associated with plants, fern spores, a genus of *Arcella* amoebae typical in freshwaters and mosses, and *Picea*/confier pollen and wood fragments (*23*). This contrasts with stratigraphic units directly underlying the mid-Holocene pedo-complex and comprising organically sterile and heavily cryoturbated sediments of Late Pleistocene age [ca. 27 to 11 ka in age; (*23*)], suggesting inhospitable environmental conditions at least until the early Holocene. We did not identify any artifacts in these deeper stratigraphic units. Therefore, the palaeoenvironmental record provides good evidence for environmental conditions at ~5 ka that were optimal for (i) human presence and use of the quarry sites, likely leading to high frequencies of artifact manufacture and discard, and (ii) low erosion and/or accumulation rates on stable hillslopes that would have facilitated artifact concentration, burial, and preservation at or near the mid-Holocene soil surface, while (iii) pre-Holocene units lack macroscopic evidence for quarry exploitation at Su-re.

With its more complex exposure and burial history, artifact TIN36 provides evidence for at least two cycles of signal buildup with initial burial at ~5.2 ka followed by a short period of re-exposure and a second burial event at ~2.38 ka. This second plateau age of TIN36 overlaps within error with the age of TIN61 of 2.36 ka, yielding a weighted mean age 2.37 ± 0.25 ka for both samples. Given the archaeological and environmental context at Su-re, the re-exposure of a previously buried and/or discarded artifact at or before ca. 2.37 ka may point to the reuse (recycling) of a previously discarded artifact by humans, thus indicating some degree of continuity in site use at Su-re. Alternatively, however, exposure and reburial may also have been caused by geomorphic processes of erosion and deposition. In contrast to the relative stability that characterized the mid-Holocene and allowed for soil formation at Su-re, sedimentary and geochronological data imply the existence of a period of landscape-scale degradation sometime between ca. 3.9 and 0.5 ka [documented and dated in (*23*)]. On the hillslopes around Su-re, erosive processes are expressed as intensive sheetwash and overland-flow events leading to soil erosion and a net lowering of the land surface (fig. S3). Consequently, these hillslope erosive processes may provide an alternative and natural explanation for the observed age-depth profile of

TIN36 with exhumation by erosion leading to re-exposure by sheetwash transport and reburial through depositional processes.

Last, two interpretations of the youngest artifact burial ages (TIN55-0.49 ± 0.12 ka and TIN56-0.45 ± 0.10 ka) with a weighted mean of 0.47 ± 0.08 ka are possible. First, the artifacts may have been produced and discarded ca. 0.47 ka. Although it is possible that these artifacts may have been produced at this time, stone tools were generally replaced by metal tools at least 2.5 ka if not earlier across most of the plateau (*20*, *40*). While additional ages are required to test this scenario, this could potentially explain the remarkable density of artifacts at Su-re (*24*, *25*). Alternatively, however, the 0.47 ka ages may also reflect the most recent time that these two artifacts were re-exposed to sunlight and subsequently buried after having been manufactured significantly earlier. This interpretation is supported by the paleoenvironmental data that point to extreme (and potentially anthropogenically induced) landscape instability during the Little Ice Age at Su-re (*23*). More specifically, aeolian sand sheets formed in the late Holocene [with depositional ages between ~0.44 and 0.64 ka, see OSL ages in (*23*)] and have been subject to intense, wind-driven erosion since then (Fig. 2C). Therefore, artifacts previously shielded by aeolian overburden (e.g., Fig. 6C) may have been excavated from their more stable positions during or before this period of landscape-scale disturbance, subjecting them to bleaching of their previously shielded surfaces followed by some transport and redeposition around 0.47 ka. These processes may also provide a reasonable explanation for the inverted age-depth profile for TIN54 (~5.45 ka). In this scenario, an older artifact may have been buried under hillslope and/or aeolian sediments before being exhumed by aeolian deflation in the last few hundred years, leading to the ongoing but still incomplete bleaching of the previously accumulated signal.

Significance for understanding artifact scatters globally

This is the first time that the OSL signal measured directly from lithic flakes has been used to determine rock burial ages for subaerially exposed discarded artifacts. As such, the method used in this study provides potential for directly dating artifact manufacture and discard on a wide geographic scale, at least where artifact lithology is suitable for the application of OSL (i.e., containing quartz or feldspar minerals). This approach has yielded the first direct ages for human occupation of this part of the Tibetan Plateau and provides an innovative method for generating chronological data for surface artifact scatters, relatively common site types that are difficult to date and generally have contributed limited archaeological information due to lack of age control.

However, our data also show that the lack of stratigraphic context when dating artifact scatters in combination with more complex age-depth profiles leaves open the possibility that artifacts may have been disturbed since being manufactured and discarded by humans. In this case, the OSL ages on the artifacts would not represent the initial artifact discard, but instead represent (one or more) subsequent events leading to the mobilization and re-exposure of a given rock surface. In this context, a range of natural and anthropogenic processes such as human- or animal-induced trampling and bioturbation [e.g., (*41*–*44*)] can potentially exhume and move gravel-sized clasts. In addition, climatically or anthropogenically induced soil degradation tends to intensify overland flow processes and aeolian deflation that can equally remove and redeposit clasts near the surface [e.g., (*9*, *45*)]. All of these processes need to be carefully considered when interpreting artifact burial ages and highlight the usefulness of accompanying geomorphic and paleoenvironmental investigations at and around the archaeological sites as common practice in geoarchaeology (*10*, *46*). In addition, artifacts may yield information on multiple bleaching and shielding events where two or more age plateaus can be observed. In this case, however, it remains inherently difficult to assign unambiguous natural (e.g., bioturbation, trampling, and sheetfloods) or anthropogenic (excavation and artifact recycling) causes to these more complex exposure and burial histories. By this logic, a burial age from an individual artifact would therefore conservatively be interpreted as representing a minimum age for human presence in the landscape and interaction with the artifact.

Methodological complexities and improvements

In this study, we determined the dose rate for each quartzite flake and associated underlying sediment sample individually to model the depth-dependent dose rate into the artifact's interior accurately and calculate plateau ages (tables S2 and S3). While radionuclide concentrations and thus dose rates are relatively constant for most of the quartzite artifacts and underlying sediment samples, one sample had significantly higher radionuclide concentrations (TIN61; table S2). EPMA and petrographic thin-section analysis revealed much higher concentrations of zircon together with other heavy minerals such as rutile and xenotime as well as elevated concentrations of interstitial kaolinite for this artifact compared to the other five samples, with a large effect on the resulting dose rate (fig. S4). In contrast, surface coatings and weathering cortexes, partly covering some of our samples, were mineralogically inconspicuous (composed of mono- and polycrystalline quartz grains), which likely had a negligible effect on the quartzite dose rates. Hence, artifact- and sample-specific dose-rate analysis in combination with microscopic techniques provides a maximum level of accuracy for the interpretation of individual plateau ages, even in macroscopically monomict lithologies such as the quartzite flakes at Su-re.

The bleaching experiments detailed above demonstrate that the Su-re quartzite bleaches rapidly, because of its relatively high translucency. For one of the thinnest flakes in this study (TIN54), bleaching through the artifact from the subaerially exposed side has been assumed to explain the inverted age-depth profile (Fig. 5F). In this study, only the underside of each quartzite flake was drilled and OSL-depth profiles with lengths between 6 and 12 mm were constructed (table S3), i.e., until the onset of a saturation plateau occurred. Obtaining profiles from the top, i.e., aerially exposed, side of each artifact could provide additional complementary information related to the exposure duration of the top side of these flakes via an OSL rock-surface exposure approach (*17*, *23*). Similarly, a rock-surface exposure dating approach could also be applied to the stepped OSL-depth profiles that were obtained from the underside of the artifacts and underlie our age-depth profiles. That is, in principle, the shape of luminescence profiles could be modeled and exposure ages could be calculated (i.e., in addition to rock-surface burial ages), and ultimately, repeated sequential events of burial and exposure to daylight could be eventually constrained (*17*). However, given the current methodological challenges associated with rock-surface exposure dating, such as calibrating the OSL-depth profiles (*16*) and the large influence of lithologically controlled transparency changes on OSL rock-surface exposure dating, also in the Su-re quartzite (*47*), we refrained from such a combined approach in the current study.

Another important aspect is the number of collectable (and dateable) artifacts and thus the robustness of the resulting archaeological and landscape chronology. Given the logistical and time constraints under which field work for this study was conducted, six out of a much larger number of collected surface clasts were identified as artifacts and investigated, and all of them yielded interpretable plateau ages. Increasing the number of samples may present a way of further testing the interpretations of complex artifact pathways and burial histories that emerge from at least two of our investigated samples. Producing large datasets from surface lithic artifact scatters seems highly feasible for two main reasons. First, many of these sites contain a large quantity of reduction by-products and may therefore be more likely to be approved for destruction in the dating process. Second, with the appropriate tools for drilling and slicing, our approach is not particularly labor-intensive and sample numbers upwards of 20 to 30 artifacts can be analyzed at relatively low cost. Also, the surface burial dating approach suggested here neither relies on the existence and analysis of calibration surfaces nor does it require age modeling of OSL-depth profiles as is the case with artifact exposure dating [e.g., (*16*)]. In combination, large enough datasets may therefore provide a statistically significant way of confirming the existing age clusters at Su-re, which will help to refine the interpretation of more complex surface burial histories, further contributing to testing the usefulness of our approach in artifact-scatter sites.

Last, rock-surface burial dating of lithic artifacts is not restricted to surface finds but can also be applied in stratified archaeological contexts, thus reducing the uncertainties resulting from more complex bleaching and burial histories that can occur in surface assemblages. In addition, directly dating deeply buried lithics avoids a range of uncertainties involved with approaches that target material only associated with these artifacts [e.g., sediment, organic material, or carbonates amenable for OSL sediment burial, radiocarbon, or U-Th dating; (*48*, *49*)]. Hence, rock-surface burial dating of lithics may hold potential for refining existing chronologies in a wide range of archaeological excavations, while fostering the integration of archaeological records from stratified sites and surface assemblages around the world.

Synthesis

The research reported here has yielded burial ages (i.e., age plateaus) for three of six lithic artifacts that are in line with conceptual models that relate luminescence signal in an artifact with a simple model of lithic reduction, discard, and surface embedding. The remaining three artifacts show age-depth profiles that can be explained by more complex geomorphic and anthropogenic processes. The oldest burial signals in our dataset yield a weighted mean age of 5.19 ± 0.31 ka, while one flake yielded a minimum age of 5.45 ± 0.54 ka. We relate this burial signal to human presence and knapping activities at Su-re during the mid-Holocene. While a burial age from an individual artifact should conservatively be interpreted as a minimum estimate, the fact that these artifacts cluster at 5.25 ka and rest atop a pedo-complex that started accumulating ca. 6.7 ka ago and have been subject to increased but spatially varying processes of sediment transport and surface erosion since ca. 3.9 ka (*23*) strongly supports our interpretation of human presence at Su-re around that time. These are the first optical ages obtained directly on discarded lithic artifacts and the oldest chronometric age constraints for human presence in the south-central sector of the Tibetan plateau.

For four of the six lithic artifacts tested, the spatially resolved surface burial ages suggest additional and more recent exposure and burial events (i.e., age plateaus at 2.37 ± 0.25 ka and 0.47 ± 0.08 ka). These events probably resulted from geomorphic processes such as erosion and redeposition during the late Holocene and the Little Ice Age (*23*), although human reuse of lithics is an alternative, though less likely explanation. In any case, our findings clearly demonstrate that surface clasts can record complex exposure and burial histories and thus transport pathways of surface artifacts in the landscape. This opens up new vistas in (geo-) archaeological and geomorphological research toward reconstructing site-specific post-depositional disturbance histories or using surface clasts as geomorphological tracers to quantify local-scale Earth-surface dynamics and thus shed new light on the integrity of archaeological surface assemblages and possibly stratified sites. Given the versatility and potential of OSL rock-surface dating, artifact surface burial dating now ideally requires rigorous testing of a range of archaeological settings in a set of contrasting landscapes. In this context, particular attention needs to be given to OSL properties of lithologies other than quartzite (e.g., also more opaque lithologies such as chert, sandstone, or granite) to ensure the presence of an exploitable OSL signal and further investigate the lithology-specific bleaching behavior that will enable the formation of well-resolved age plateaus in centimeter-scale artifacts. If successful, OSL rock-surface burial dating then has the potential to become widely applicable, shining new light on the production and burial history of lithic artifacts in a diverse range of archaeological contexts.

MATERIALS AND METHODS

All sample preparation was performed in a red-lit laboratory. To measure OSL-depth profiles, cores (8.5 mm diameter) were drilled using a water-cooled diamond core drill. The cores (>20 mm in length) were then sliced in 1-mm increments using a diamond wafering blade (0.3 mm thick) mounted on a Buehler low-speed saw, yielding slices that had an average thickness of 0.66 ± 0.07 mm. The slices were then crushed with a mortar and pestle, and the resulting grains were sieved to retain those with a diameter of 90 to 250 μm. The grains were then mounted on stainless steel discs using a 5-mm mask (~600 grains per aliquot) and measured using a Risø TL/OSL DA-20 reader (*50*). Aliquots were stimulated using blue light-emitting diodes (LEDs) (470 ± 30 nm) following infrared (IR) (875 nm) stimulations in a post-IR OSL approach to ensure the purity of quartz OSL signal. Photons were measured using an Electron Tubes Ltd. 9635 photomultiplier tube, and the ultraviolet OSL emissions were measured through 7.5 mm of Hoya U-340 filter. IR stimulations were performed for 100 s at 50°C, and blue stimulations were performed for 100 s at 125°C. The signal was calculated by summing the first 1 s of signal minus a background calculated from the last 20 s of stimulation. Laboratory irradiations were given using a calibrated $^{90}Sr/^{90}Y$ beta source mounted on the Risø TL/OSL reader. De values for dating artifact discard were measured using a modified single-aliquot regenerative-dose (SAR) procedure (*51*) with a preheat of 220°C (10 s) for natural/regenerative dose and test dose, and post-IR OSL measurement was used to estimate De values. Standard tests of SAR suitability, including a recycling ratio (unity ± 2σ) and recuperation test (5%), were included. Dose recoveries yielded consistent measured/given dose ratios (1.01 ± 0.02, n = 24) and recycling ratios (1.02 ± 0.02, n = 24), and negligible recuperation

(0.007 ± 0.002, n = 24), indicating that the SAR procedure can be used to reliably measure known radiation doses for Su-re quartzite samples. De values were measured for between four and six aliquots per slice. Some slices showed significant dispersion in aliquot De values. To target the aliquots that best reflect burial, the aliquot De data that passed standard SAR suitability tests were analyzed using the homogeneity test of Galbraith (*39*) to identify statistically consistent populations of De values. Where all aliquots from a slice yielded a homogeneous population, the weighted mean was calculated. Where not all aliquots contributed to a homogeneous population of De values, those outlier aliquots were rejected, and a weighted mean was calculated for the homogeneous population of De values. For seven slices (TIN54 slice 5 and TIN59 slices 1 to 6), no homogeneous population could be identified. For these slices, extreme outliers (outlier De an order of magnitude larger than the rest) and aliquots that failed rejection criteria were removed, and a weighted mean was calculated for the remaining De values. From all measured aliquots, 40 (of 248) aliquots were rejected for either (i) not yielding a De value, (ii) failing a SAR suitability test, or (iii) yielding an outlier De value. Weighted mean De values for each slice were calculated using the CAM, except for those slices with aliquots that yielded negative De values. In those cases, the unlogged CAM (*38*) was used (fig. S5 and table S3).

A full SAR procedure was not used during the bleaching experiment, during which only Ln/Tn values were measured. To convert Ln/Tn values from bleaching experiments to De values ex post facto, a lithology-specific SGC (*34*) was created. To do this, dose-response curves were measured using the same measurement sequence and parameters for 372 aliquots of Su-re quartzite material and the arithmetic average and SD of Lx/Tx values for a given regenerative dose were calculated to create a lithology-specific standardized Lx/Tx value. These were then fitted with an exponential function to generate a SGC, onto which Ln/Tn values from the bleaching experiment were projected to calculate De values.

The dose rates experienced by samples were estimated using two independent methods: (i) measuring and modeling quartzite and sediment material and (ii) aluminum oxide dosimetry. The total environmental dose rate was determined for each sample individually and the radionuclide concentration and thus dose rate from within each quartzite artifact as well as from the underlying sediment has been accounted for. For each quartzite sample, a drill core was obtained next to the OSL drill hole and U, Th, K, and Rb concentrations were determined using inductively coupled plasma optical emission spectrometry (ICP-OES) and ICP mass spectrometry (ICP-MS) at Activation Laboratories LTD, Canada (table S2). Sediment samples underlying artifacts were collected during field work and measured using a combination of GM-25-5 beta counting (*52*) and thick-source alpha counting. Corrections were made for beta attenuation (*53*) and the conversion factors of Guérin *et al.* (*54*) were used to calculate beta and gamma dose rates. For quartzite samples, a water content of 0 was used. For sediment samples, a water content of 5% was used to calculate dose rate attenuation by water and a 50% uncertainty was applied to allow for past variations in the moisture. In this way, sample-specific rock and sediment beta and gamma dose rates were determined. However, due to the large penetration depth of gamma rays in sediment (ca. 30 to 40 cm), dose-rate heterogeneities could be expected if clasts of rocks are embedded beneath the sampled artifacts. Consequently, we calculated a weighted mean gamma dose rate from all six sediment samples (using the SD for error propagation) and used this weighted average sediment gamma dose rate. Thus, the dose rates used for spatially resolved dose rate modeling (fig. S6) for each artifact were (i) the sample-specific beta and gamma dose rates for rock samples, (ii) the sample-specific moisture corrected beta dose rate for each sediment sample, and (iii) the moisture corrected weighted average gamma dose rate derived from all of the sediment samples (table S2).

The dose rate experienced by the targeted sample slices includes differing contributions from the rock itself, the underlying sediments, and the overlying air (fig. S6). Using the depth into rock surface of each slice and the geometry of each artifact, the equations of Aitken (*32*) (appendix H) were used to calculate spatially relevant beta and gamma dose rates for each slice. The beta dose rate in the rock due to the underlying sediment was calculated as follows

$$\dot{D}^{rock}_{\beta,sed} = 0.5\,\dot{D}_{\beta,sed}\,e^{-ax}$$

where $\dot{D}_{\beta,sed}$ (Gy/ka) is the measured beta dose rate of the sediment, a (mm^{-1}) is the beta linear attenuation coefficient in rock, and x (mm) is the depth into the rock from the rock-sediment interface (fig. S6A). The beta contribution to the rock due to itself is given by

$$\dot{D}^{rock}_{\beta,rock} = \dot{D}_{\beta,rock}\{1 - 0.5(e^{-ax} + e^{-a(h-x)})\}$$

where $\dot{D}_{\beta,rock}$ (Gy/ka) is the measured beta dose rate of the rock and h (mm) is the artifact thickness (fig. S6A). The gamma dose rate in the rock due to the underlying sediment was calculated as follows

$$\dot{D}^{rock}_{\gamma,sed} = 0.5\,\dot{D}_{\gamma,sed}\,e^{-bx}$$

where $\dot{D}_{\gamma,sed}$ (Gy/ka) is the gamma dose rate of the sediment and b (mm^{-1}) is the gamma linear attenuation coefficient in rock (fig. S6A). The gamma contribution to the rock due to itself is given by

$$\dot{D}^{rock}_{\gamma,rock} = \dot{D}_{\gamma,rock}\{1 - 0.5(e^{-bx} + e^{-b(h-x)})\}(m + m - 1)(n + n - 1)$$

where $\dot{D}_{\gamma,rock}$ (Gy/ka) is the measured gamma dose rate of the rock and m and n are the fractional doses from Aitken (*32*) (table H.1) calculated for the length and width, respectively, of each artifact (fig. S6A). The values of a (1.9 mm^{-1}) and b (0.2 mm^{-1}) calculated by Sohbati *et al.* (*11*) were used, which assume a rock density of 2.6 g cm^{-3}. Variations in the total dose rate were calculated in 0.5-mm increments into the buried rock surface (fig. S6B). Total effective dose rates for each ~0.7-mm-thick slice were calculated using the sample-specific total dose rates calculated for appropriate depth intervals, plus a cosmic-ray dose rate (0.41 ± 0.04 Gy/ka) calculated following Prescott and Hutton (*55*) and an internal (intra-quartz grain) alpha dose rate of 0.03 ± 0.01 Gy/ka (*56*). The average rock-sediment interface dose rate is 3.51 ± 0.09 Gy/ka.

Quartz grain external alpha dose rate contributions were considered but were not included in the artifact-specific total dose rates (note that this quartz grain external alpha dose rate is still an artifact internal dose rate and thus sample specific). Because the bulk of the quartzite artifacts comprises homogeneous quartz grains with rare occurrences of heavy minerals with higher U and Th concentrations (serving as alpha emitters; fig. S4), most quartz grains are surrounded by other quartz grains. Consequently, the alpha contribution to the vast majority of quartz grains would already be considered by the quartz grain internal alpha dose rate included in total dose rate

calculation (see above). As an example, consider sample TIN61, which has the highest U and Th concentrations and the highest concentration of heavy minerals of all measured samples (Fig. 4B). Figure S4B shows that heavy minerals comprise approximately 3% of the measured area, with the remaining area comprising quartz grains. Given the small range of alpha particles (20 to 30 μm in quartz), the grain size of quartz grains (~200 μm), and the small and uneven distribution of heavy minerals within the sample, the averaged external alpha contribution to the dose rate would be an insignificant 0.01 Gy/ka for a situation depicted in fig. S4B. Note that fig. S4B shows an area of very high heavy mineral concentration even within sample TIN61 and thus likely represents a maximum external alpha dose rate scenario. Furthermore, considering fig. S4B, heavy minerals are not evenly distributed, and thus, the addition of an external heavy mineral–derived alpha dose rate would not be appropriate for the vast majority of grains. In addition, the small populations of grains that would have experienced elevated external alpha dose rates due to their proximity to higher concentrations of heavy minerals could be related to the high-De outliers in fig. S5. These outliers have been removed from weighted mean slice De calculations, thereby circumventing the uncertain effects of the external alpha dose rate on age calculation.

The weighted mean slice De value was then divided by the spatially resolved dose rate for each slice to calculate an OSL burial age for each slice (table S1). Plateaus in the OSL age-depth data were identified using the homogeneity test of Galbraith (*39*) as follows: (i) Age-depth profiles were created for each artifact sample. (ii) The slices' ages were then analyzed with the homogeneity test as follows: slices 1 + 2, slices 1 + 2 + 3, slices 1 + 2 + 3 + 4, and so on, until the homogeneity test yielded a failed result ($P < 0.05$). The plateau was then considered to be from slice 1 to the deepest slice that passed the homogeneity test. (iii) The process was repeated from the first slice to fail the homogeneity test and deeper into the core to identify potential deeper plateaus. Where a statistically homogeneous age plateau was identified, a weighted mean plateau age was calculated using the CAM. One sample (TIN61) exhibited a clear plateau that did not comprise a homogeneous population of ages according to Galbraith (*39*). For this sample, the weighted mean was calculated using the CAM.

Aluminum oxide dosimeters were placed under a series of similar-sized natural quartzite samples in the Su-re quarry site in 2014. Samples were left for 1.667 years before collection in 2016. Only one aluminum oxide dosimeter could be recovered, which was measured using the same Risø TL/OSL reader used for De measurement. The De of the dosimeter was measured using a SAR procedure that included a test dose of 1 s of beta stimulation (0.10 Gy), regenerative and test dose preheats of 80°C for 10 s, 60-s blue LED stimulations at 50°C, and a 200-s optical bleach at 30°C following each test dose cycle. This dosimeter yielded a De value of 0.005 ± 0.002 Gy after 1.667 years of exposure, indicating a dose rate of 3.09 ± 1.24 Gy/ka, supporting the dose rate derived from laboratory measurement and modeling.

In addition, thin-section petrography was conducted on selected artifacts using a polarization microscope and the electron probe microanalyzer. The JEOL Superprobe 8100 electron probe microanalyzer (analytical conditions: 15-kV voltage and 10-nA current) was used to generate backscattered electron (BSE) images and identify the minerals using the energy-dispersive analytical system (EDS). These investigations revealed that all artifacts are low-grade metamorphic sandstones composed of quartz and rare zircons (fig. S4A). One sample (TIN61) revealed a higher concentration of heavy minerals such as pyrite, zircon, Nb-bearing rutile, and xenotime, and this sample also showed a higher abundance of kaolinite domains (fig. S4B). BSE images and EDS analyses also revealed that, in both samples, kaolinite domains occur interstitially between quartz grains. Although sample TIN61 shows elevated K_2O and Rb contents (ICP-OES and ICP-MS data; table S2), no mineral grains into which K and Rb are typically incorporated such as muscovite or K-feldspar were identified. EDS analysis yielded low K_2O contents (<0.1 weight %) within the kaolinite domains. It is possible that, within these kaolinite domains, very fine grained illite is present, which acts as a Rb and K carrier, but was too fine-grained to be resolved. We suggest that such fine-grained (crypto-crystalline) illites are the source for the elevated Rb and K concentrations observed in TIN61, while the numerous zircons and xenotimes are responsible for the high U and Th concentrations, collectively causing the high dose rate of TIN61 (compare table S2).

SUPPLEMENTARY MATERIALS

Supplementary material for this article is available at http://advances.sciencemag.org/cgi/content/full/7/23/eabb3424/DC1

REFERENCES AND NOTES

1. E. C. Harris, The laws of archaeological stratigraphy. *World Archaeol.* **11**, 111–117 (1979).
2. G. Lucas, *Understanding the Archaeological Record* (Cambridge Univ. Press, 2012).
3. D. Richter, Advantages and limitations of thermoluminescence dating of heated flint from Paleolithic sites. *Geoarchaeology* **22**, 671–683 (2007).
4. I. Liritzis, N. Laskaris, Fifty years of obsidian hydration dating in archaeology. *J. Non Cryst. Solids* **357**, 2011–2023 (2011).
5. P. C. Fanning, S. J. Holdaway, E. J. Rhodes, T. G. Bryant, The surface archaeological record in arid Australia: Geomorphic controls on preservation, exposure, and visibility. *Geoarchaeology* **24**, 121–146 (2009).
6. M. S. Bisson, A. Nowell, C. Cordova, M. Poupart, C. Ames, Dissecting palimpsests in a Late Lower and Middle Paleolithic flint acquisition site on the Madaba Plateau, Jordan. *Quat. Int.* **331**, 74–94 (2014).
7. B. Davies, S. J. Holdaway, P. C. Fanning, Modelling the palimpsest: An exploratory agent-based model of surface archaeological deposit formation in a fluvial arid Australian landscape. *Holocene* **26**, 450–463 (2016).
8. B. Davies, S. J. Holdaway, Windows on the past? Perspectives on accumulation, formation, and significance from an Australian Holocene lithic landscape. *Mitteilungen der Gesellschaft für Urgeschichte* **26**, 125–152 (2017).
9. J. Knight, A. Zerboni, Formation of desert pavements and the interpretation of lithic-strewn landscapes of the central Sahara. *J. Arid Environ.* **153**, 39–51 (2018).
10. P. C. Fanning, S. J. Holdaway, E. J. Rhodes, A new geoarchaeology of Aboriginal artifact deposits in western NSW, Australia: Establishing spatial and temporal geomorphic controls on the surface archaeological record. *Geomorphology* **101**, 524–532 (2008).
11. R. Sohbati, A. S. Murray, N. Porat, M. Jain, U. Avner, Age of a prehistoric "Rodedian" cult site constrained by sediment and rock surface luminescence dating techniques. *Quat. Geochronol.* **30**, 90–99 (2015).
12. S. al Khasawneh, A. Murray, F. Abudanah, A first radiometric chronology for the Khatt Shebib megalithic structure in Jordan using the luminescence dating of rock surfaces. *Quat. Geochronol.* **49**, 205–210 (2019).
13. J. Feathers, G. M. More, P. S. Quinteros, J. E. Burkholder, IRSL dating of rocks and sediments from desert geoglyphs in coastal Peru. *Quat. Geochronol.* **49**, 177–183 (2019).
14. A. R. Simms, R. DeWitt, P. Kouremenos, A. M. Drewry, A new approach to reconstructing sea levels in Antarctica using optically stimulated luminescence of cobble surfaces. *Quat. Geochronol.* **6**, 50–60 (2011).
15. G. T. H. Jenkins, G. A. T. Duller, H. M. Roberts, R. C. Chiverrell, N. F. Glasser, A new approach for luminescence dating glaciofluvial deposits—High precision optical dating of cobbles. *Quat. Sci. Rev.* **192**, 263–273 (2018).
16. L. A. Gliganic, M. C. Meyer, R. Sohbati, M. Jain, S. Barrett, OSL surface exposure dating of a lithic quarry in Tibet: Laboratory validation and application. *Quat. Geochronol.* **49**, 199–204 (2019).
17. T. Freiesleben, R. Sohbati, A. Murray, M. Jain, S. Al Khasawneh, S. Hvidt, B. Jakobsen, Mathematical model quantifies multiple daylight exposure and burial events for rock surfaces using luminescence dating. *Radiat. Meas.* **81**, 16–22 (2015).

18. P. J. Brantingham, J. W. Olsen, G. B. Schaller, Lithic assemblages from the Chang Tang region, northern Tibet. *Antiquity* **75**, 319–327 (2001).
19. M. Aldenderfer, Y. Zhang, The prehistory of the Tibetian plateau to the seventh century A.D.: Perspectives and research from China and the west since 1950. *J. World Prehist.* **18**, 1–55 (2004).
20. J. D'Alpoim Guedes, M. Aldenderfer, The Archaeology of the early Tibetan plateau: New research on the initial peopling through the early Bronze Age. *J. Archaeol. Res.* **27**, 1–54 (2019).
21. B. Y. Yuan, W. W. Huang, D. Zhang, New evidence for human occupation of the northern Tibetan Plateau, China during the Late Pleistocene. *Chin. Sci. Bull.* **52**, 2675–2679 (2007).
22. M. C. Meyer, M. S. Aldenderfer, Z. Wang, D. L. Hoffmann, J. A. Dahl, D. Degering, W. R. Haas, F. Schlütz, Permanent human occupation of the central Tibetan Plateau in the early Holocene. *Science* **355**, 64–67 (2017).
23. M. C. Meyer, L. A. Gliganic, J. H. May, S. Merchel, G. Rugel, F. Schlütz, M. S. Aldenderfer, K. Krainer, Landscape dynamics and human-environment interactions in the northern foothills of Cho Oyu and Mount Everest (southern Tibet) during the Late Pleistocene and Holocene. *Quat. Sci. Rev.* **229**, 106127 (2020).
24. S. S. Zhang, Newly discovery of Paleolithic from Tingri, Tibet, in *Chinese Academy of Sciences Multidisciplinary Expedition of Qomolangma (1966–1968): Quaternary Geology* (Science Press, 1976), pp. 105–109.
25. E. Tong, Xi zang gao yuan shang de shou fu [Hand axe from the Tibetan plateau]. *Kaogu* **9**, 822–826 (1989).
26. M. Oppitz, Myths and facts: Reconsidering some data concerning the clan history of the Sherpas. The Sherpa Society 1, 121–131 (1974); http://www.dspace.cam.ac.uk/handle/1810/227209. (accessed 5th January 2020).
27. R. Gautama, A. K. Thapa-Magar, *Tribal Ethnography of Nepal* (Book Faith India, 1994), vol. 2.
28. T. Jiang, J. C. Aitchison, X. Wan, The youngest marine deposits preserved in southern Tibet and disappearance of the Tethyan Ocean. *Gondw. Res.* **32**, 64–75 (2016).
29. K. S. Brown, C. W. Marean, A. I. Herries, Z. Jacobs, C. Tribolo, D. Braun, D. L. Roberts, M. C. Meyer, J. Bernatchez, Fire as an engineering tool of early modern humans. *Science* **325**, 859–862 (2009).
30. D. J. Huntley, D. I. Godfrey-Smith, M. L. W. Thewalt, Optical dating of sediments. *Nature* **313**, 105–107 (1985).
31. E. J. Rhodes, Optically stimulated luminescence dating of sediments over the past 200,000 years. *Annu. Rev. Earth Planet. Sci.* **39**, 461–488 (2011).
32. M. J. Aitken, *Thermoluminescence Dating* (Academic Press, 1985).
33. R. Sohbati, A. S. Murray, M. S. Chapot, M. Jain, J. Pederson, Optically stimulated luminescence (OSL) as a chronometer for surface exposure dating. *J. Geophys. Res.* **117**, B09202 (2012).
34. H. M. Roberts, G. A. T. Duller, Standardised growth curves for optical dating of sediment using multiple-grain aliquots. *Radiat. Meas.* **38**, 241–252 (2004).
35. World Map of Global Horizontal Irradiation, SolarGIS (2013); https://commons.wikimedia.org/w/index.php?title=File:SolarGIS-Solar-map-World-map-en.png&oldid=127621989 (last accessed 5 Nov. 2019).
36. H. Liang, R. Zhang, J. Liu, Z. Sun, X. Cheng, Estimation of hourly solar radiation at the surface under cloudless conditions on the Tibetan Plateau using a simple radiation model. *Adv. Atmos. Sci.* **29**, 675–689 (2012).
37. R. F. Galbraith, R. G. Roberts, G. M. Laslett, H. Yoshida, J. M. Olley, Optical dating of single and multiple grains of quartz from Jinmium rock shelter, northern Australia: Part I, experimental design and statistical models. *Archaeometry* **41**, 339–364 (2012).
38. L. J. Arnold, R. G. Roberts, R. F. Galbraith, S. B. DeLong, A revised burial dose estimation procedure for optical dating of youngand modern-age sediments. *Quat. Geochronol.* **4**, 306–325 (2009).
39. R. Galbraith, A simple homogeneity test for estimates of dose obtained using OSL. *Anc. TL* **21**, 75–77 (2003).
40. H. Wei, On the early metal objects and early Metal Age in Tibet. *Chin. Archaeol.* **16**, 91–96 (2016).
41. W. R. Wood, D. L. Johnson, A survey of disturbance processes in archaeological site formation, in *Advances in Archaeological Method and Theory*, M. B. Schiffer, Ed. (Academic Press, 1978), vol. 1, pp. 315–381.
42. P. Villa, J. Courtin, The interpretation of stratified sites: A view from underground. *J. Archaeol. Sci.* **10**, 267–281 (1983).
43. P. Goldberg, D. T. Nash, M. D. Petraglia, *Formation Processes in Archaeological Context* (Prehistory Press, 1993).
44. M. Navazo, C. Díez, Redistribution of archaeological assemblages in plowzones. *Geoarchaeology* **23**, 323–333 (2008).
45. D. E. Lewarch, M. J. O'Brien, The expanding role of surface-assemblages in archaeological research. *Adv. Archaeol. Method Theory* **4**, 297–342 (1981).
46. P. Goldberg, R. I. Macphail, *Practical and Theoretical Geoarchaeology* (Blackwell Publishing, 2008).
47. M. C. Meyer, L. A. Gliganic, M. Jain, R. Sohbati, D. Schmidmair, Lithological controls on light penetration into rock surfaces - implications for OSL and IRSL surface exposure dating. *Radiat. Meas.* **120**, 298–304 (2018).
48. M. J. Aitken, Luminescence dating, in *Chronometric Dating in Archaeology* (Springer, 1997), pp. 183–216.
49. R. G. Roberts, Z. Jacobs, Dating in landscape archaeology, in *Handbook of Landscape Archaeology* (Left Coast Press, 2008), vol. 1, pp. 347–364.
50. L. Bøtter-Jensen, K. J. Thomsen, M. Jain, Review of optically stimulated luminescence (OSL) instrumental developments for retrospective dosimetry. *Radiat. Meas.* **45**, 253–257 (2010).
51. A. S. Murray, A. G. Wintle, Luminescence dating of quartz using an improved single-aliquot regenerative-dose protocol. *Radiat. Meas.* **32**, 57–73 (2000).
52. L. Bøtter-Jensen, V. Mejdahl, Assessment of beta dose-rate using a GM multicounter system. *Int. J. Rad. Appl. Instrum. D* **14**, 187–191 (1988).
53. V. Mejdahl, Thermoluminescence dating: Beta-dose attenuation in quartz grains. *Archaeometry* **21**, 61–72 (1979).
54. G. Guérin, N. Mercier, G. Adamiec, Dose-rate conversion factors: Update. *Anc. TL* **29**, 5–8 (2011).
55. J. R. Prescott, J. T. Hutton, Cosmic ray contributions to dose rates for luminescence and ESR dating: Large depths and long-term time variations. *Radiat. Meas.* **23**, 497–500 (1994).
56. J. M. Bowler, H. Johnston, J. M. Olley, J. R. Prescottk, R. G. Roberts, W. Shawcross, N. A. Spooner, New ages for human occupation and climatic change at Lake Mungo, Australia. *Nature* **421**, 837–840 (2003).

Acknowledgments: The lithics were illustrated by L. F. Blanco and E. Huerta of University of California, Davis. We thank R. Sohbati and M. Jain for fruitful discussion of the OSL data and K. Krainer for help with petrographic thin-section analysis. We thank T. Rittenour and W. Amidon and one anonymous reviewer for constructive comments that helped to improve this paper. **Funding:** This work was funded by Austrian Science Fund grants to L.A.G. (FWF grant M2121-G25) and M.C.M. (FWF grant 24924-G19). **Author contributions:** L.A.G. and M.C.M. were responsible for conceiving the study and writing the manuscript with contributions from J.-H.M. and M.S.A. L.A.G., M.C.M. and J.-H.M. were responsible or coresponsible for data interpretation and developed the conceptual model shown in Figs. 3 and 6. L.A.G. and M.C.M. were responsible for luminescence dating. M.S.A. analyzed and described the artifacts. Field work was conducted by M.C.M., L.A.G., J.-H.M., and M.S.A. P.T. was responsible for the electron microprobe analysis. **Competing interests:** The authors declare that they have no competing interests. **Data and materials availability:** All data needed to evaluate the conclusions in the paper are present in the paper and/or the Supplementary Materials.

Submitted 20 February 2020
Accepted 19 April 2021
Published 2 June 2021
10.1126/sciadv.abb3424

Citation: L. A. Gliganic, M. C. Meyer, J.-H. May, M. S. Aldenderfer, P. Tropper, Direct dating of lithic surface artifacts using luminescence. *Sci. Adv.* **7**, eabb3424 (2021).

Direct dating of lithic surface artifacts using luminescence

Luke Andrew Gliganic, Michael Christian Meyer, Jan-Hendrik May, Mark Steven Aldenderfer and Peter Tropper

Sci Adv **7** (23), eabb3424.
DOI: 10.1126/sciadv.abb3424